



# Overcoming of energy barrier for irreversible magnetization in nanocomposite magnets



Zhu-bai Li<sup>a,b</sup>, Ying Zhang<sup>b,\*</sup>, Bao-gen Shen<sup>b,\*</sup>, Ming Zhang<sup>b</sup>, Feng-xia Hu<sup>b</sup>, Ji-rong Sun<sup>b</sup>

<sup>a</sup> Key Laboratory of Integrated Exploitation of Bayan Obo Multi-Metal Resources, Inner Mongolia University of Science and Technology, Baotou 014010, China

<sup>b</sup> State Key Laboratory for Magnetism, Institute of Physics, Chinese Academy of Sciences, Beijing 100190, China

## ARTICLE INFO

### Article history:

Received 23 April 2016

Received in revised form

24 July 2016

Accepted 30 August 2016

Available online 30 August 2016

### Keywords:

Nanocomposite magnets

Energy barrier

Magnetization reversal

Coercivity

## ABSTRACT

The irreversible magnetization occurs mainly in hard grains in nanocomposite magnets, and the domain wall involves a little part of defect region in irreversible magnetization due to the self-interaction. The investigation on thermal activation shows that the defect region involved in domain wall becomes narrower due to the TiNb addition in Pr<sub>2</sub>Fe<sub>14</sub>B/α-Fe magnets. The defect region augments the energy density in the negative direction of domain wall to overcome the energy barrier of perfect hard region. The soft phase, exchange-coupled with defect region at hard grain outer-layer, promotes magnetization reversal in defect region by exchange coupling. While the defect region plays a role as a ladder to overcome the energy barrier, resulting in the decrease of coercivity more or less depending upon the width and anisotropy of defect region.

© 2016 Elsevier B.V. All rights reserved.

## 1. Introduction

Giant energy product is expected in nanocomposite magnets which combine the merits of magnetically soft and hard phases while maintaining a uniform magnetic behavior [1–6]. However, the applied field promotes magnetization reversal more easily in soft phase, and magnetization reversal behavior is incoherent near the interface in irreversible magnetization [7,8]. A slight change of interfacial structure results probably in a large variation in coercivity [9,10]. The atomic interdiffusion [11–13], the aggregation of nonmagnetic elements at the interface [14], the graded or rigid interface can strongly affect the magnetization reversal [15,16]. It is interesting to know how the magnetization reversal undergoes near the interface and what significantly affects the coercivity in nanocomposite magnets.

Coercivity is the resistance to demagnetization and determined by the irreversible magnetization [17,18], which occurs at grain outer-layer for reversed domain nucleation [19,20]. In magnetization reversal, the applied field promotes the magnetic disorder [21], and the nucleation of reversed domain is actually incoherent magnetization behavior accompanied by the increase of domain wall energy [22]. The smaller domain wall implies more incoherence and higher disorder degree of magnetic moments with high exchange energy density, and the coercivity is strongly dependent on the domain wall size in irreversible magnetization

[18]. So the coercivity is closely related with the evolution of energy in the nucleation process of reversed domain wall. Thermal activation is irreversible magnetization resulting from the overcoming of energy barrier [23,24], which provides a novel method to investigate the coercivity from the angle of energy competition [18]. The addition of nonmagnetic or refractory elements may perfect grain boundary and regulate the behavior of magnetization reversal [13,25]. Here we probe the variation of domain wall size for Pr<sub>2</sub>Fe<sub>14</sub>B/α-Fe magnets with the doping of Ti and Nb. It is expected that these investigation could contribute to the substantial understanding on the energy evolution for the nucleation of domain wall in determining coercivity.

## 2. Experimental procedure

The ingots with nominal compositions varying from Pr<sub>9</sub>Fe<sub>85.5</sub>B<sub>5.5</sub> to Pr<sub>9</sub>Fe<sub>82.5</sub>Ti<sub>2</sub>Nb<sub>1</sub>B<sub>5.5</sub> were prepared by arc melting method under an argon gas. The ingot was re-melted by induction melting in quartz tube and the ribbons were obtained by ejecting the melt onto the surface of a rotating copper wheel by pressurized argon. The wheel surface was polished under rotating state using the 1000-grit paper. The optimum surface velocity of copper wheel was 21.5 m/s for Pr<sub>9</sub>Fe<sub>85.5</sub>B<sub>5.5</sub>, and that was decreased for adapting the doping of the refractory metal TiNb in order to optimize coercivity and the squareness of hysteresis loop. The phase constitution was examined by x-ray diffraction (XRD). Magnetic measurements were performed using superconducting quantum interference device (SQUID) vibrating sample magnetometer

\* Corresponding authors.

E-mail addresses: [zhangy@iphy.ac.cn](mailto:zhangy@iphy.ac.cn) (Y. Zhang), [shenbg@iphy.ac.cn](mailto:shenbg@iphy.ac.cn) (B.-g. Shen).

(VSM). The microstructure and domain structure were observed using a Tecnai F20 Transmission Electron Microscopy (TEM), and the domain structures were recorded using Fresnel mode with the objective-lens off.

### 3. Results and discussion

The hybrid structure containing isotropic  $\text{Pr}_2\text{Fe}_{14}\text{B}$  and  $\alpha\text{-Fe}$  phases is confirmed by XRD in these Pr-Fe-B ribbons (shown in Fig. 1). Due to the broadening of diffraction peaks some peaks are nearly overlaps in the XRD pattern, such as the  $\text{Pr}_2\text{Fe}_{14}\text{B}$  (006) and  $\alpha\text{-Fe}$  (110) peaks. In nanocomposites the peaks at  $\alpha\text{-Fe}$  (110) position are much stronger than that in  $\text{Pr}_9\text{Fe}_{85.5}\text{B}_{5.5}$  ribbons, which should be attributed to the larger amount of  $\alpha\text{-Fe}$  phase. Owing to nearly the same diffraction peak intensities near (110) position the amounts of  $\alpha\text{-Fe}$  are assumed to be the same among these nanocomposites. Using Jade software it is estimated that the average grain sizes are all in the range of 20–30 nm. Fig. 2 shows the hysteresis loops for the optimally melt-spun ribbons, and that of nanocrystalline  $\text{Pr}_{11}\text{Fe}_{83.5}\text{B}_{5.5}$  ribbons are also shown for a comparison. With the increase of TiNb atomic percent, the coercivity increases simultaneously. Table 1 lists the magnetic properties and the optimal wheel surface velocity in melt spinning for these ribbons. Coercivity was obtained by performing standard

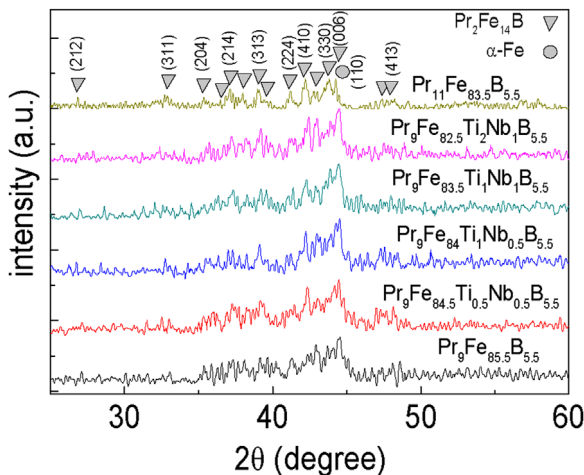


Fig. 1. The XRD patterns of all samples.

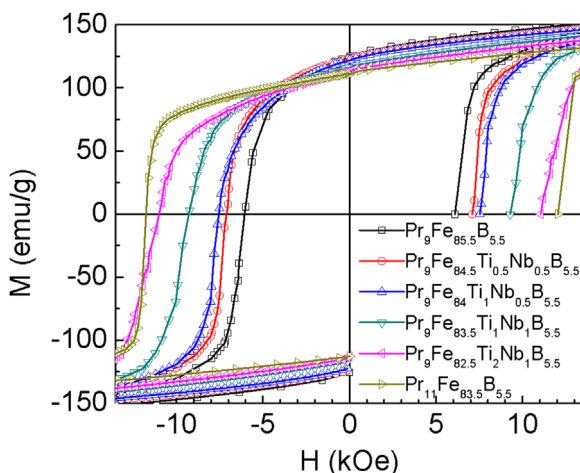


Fig. 2. The hysteresis loops for nanocomposite and nanocrystalline magnets at temperature of 300 K.

Table 1

Magnetic properties at temperature of 300 K for Pr-Fe-B ribbons prepared with the optimal wheel surface velocity.

Composition	Surface velocity (m/s)	$H_c$ (kOe)	$M_r$ (emu/g)	Squareness	$(BH)_{\max}$ (MGoe)
$\text{Pr}_9\text{Fe}_{85.5}\text{B}_{5.5}$	21.5	6.07	124.1	0.767	21.13
$\text{Pr}_9\text{Fe}_{84.5}\text{Ti}_{0.5}\text{Nb}_{0.5}\text{B}_{5.5}$	16	7.10	123.4	0.785	22.90
$\text{Pr}_9\text{Fe}_{84}\text{Ti}_1\text{Nb}_{0.5}\text{B}_{5.5}$	14	7.54	121.8	0.754	21.32
$\text{Pr}_9\text{Fe}_{83.5}\text{Ti}_1\text{Nb}_1\text{B}_{5.5}$	12	9.27	116.0	0.778	22.30
$\text{Pr}_9\text{Fe}_{82.5}\text{Ti}_2\text{Nb}_1\text{B}_{5.5}$	10	10.99	112.7	0.759	21.45
$\text{Pr}_{11}\text{Fe}_{83.5}\text{B}_{5.5}$	24	11.79	110.9	0.834	22.97

demagnetization measurements and determined in the irreversible magnetization [18]. Thermal activation, resulting from the overcoming of an energy barrier with the driving of thermal fluctuation [26,27], is the irreversible magnetization and reflects the activation size dependence of coercivity [18,28]. The magnetization behaviors of thermal activation were obtained in the following method. Firstly, the sample was magnetized to saturation in the positive direction. Next, applied a negative field, kept the field fixed for 1200 s of waiting time and then increased it at a low sweep rate of 10 Oe/s. According to the tangents of magnetization curve the aftereffect field is obtained (shown in Fig. 3(a)), which corresponds to the fluctuation field  $H_f$  [26]. The activation size  $d_{\text{active}}$  is obtained by the formula,  $d_{\text{active}} = \sqrt[3]{v}$ , where activation volume  $v = k_B T / H_f M_s$  ( $k_B = 1.38 \times 10^{-23}$  J/K,  $T = 300$  K,  $M_s = 1.55$  T).

In the critical behavior of irreversible process, domain wall energy approaches nearly to a maximum, domain wall size reduces nearly to the minimum, and thermal activation occurs mainly in hard grains [18]. The activation size is actually the minimum unit of self-interaction swept in the thermal activation [29,30], which could be regarded as the reversed domain wall size in the critical behavior [18,30]. The ideal domain wall size  $\delta_m$  is about 3.7 nm for  $\text{Pr}_2\text{Fe}_{14}\text{B}$  magnets [26]. But as shown in Fig. 3(b), all of the activation sizes are a little larger than the ideal size, and the doping of Ti and Nb leads to the decrease of  $d_{\text{active}}$ . There are three regions near the interface, i.e., perfect hard region, defect region (transition region) and soft region [7]. The nucleation of reversal domain begins in defect region at grain boundary, but irreversible magnetization reversal occurs mainly in perfect hard region [19]. So it is the exchange coupling between the defect and perfect hard regions in the activation volume that promotes magnetization reversal and lowers the barrier of nucleation in perfect hard region [18]. The decrease of  $d_{\text{active}}$  suggests that the volume fraction of defect and/or soft region in domain wall is reduced, the exchange coupling length is decreased, and therefore magnetization reversal becomes more incoherent, which seems to be responsible for the coercivity enhancement.

Henkel plots, defined as  $\delta m = [2M_r(H) + M_d(H)] / M_r - 1$  [31], could reveal the exchange coupling effect in nanoscale isotropic magnets. Here  $M_r(H)$  and  $M_d(H)$  are the initial remanence and demagnetization remanence, respectively, and  $M_r$  is the saturation remanence. The positive  $\delta m$  value, indicating a strong exchange coupling between grains over the dipolar effect, doesn't decrease for nanocomposites with TiNb doping (shown in Fig. 4). But the negative maximum of  $\delta m$  value decreases, implying the weakening of dipolar effect. In nanocrystalline  $\text{Pr}_{11}\text{Fe}_{83.5}\text{B}_{5.5}$ , the larger maximum of  $\delta m$  is due to the rather low amount of soft phase [32]. This fact suggests that the doping of TiNb doesn't cause weakening effect of exchange coupling and the variation of  $\delta m$  value is not responsible for the lowering of the barrier of nucleation in perfect hard region.

Suppose that the exchange constants are the same near the interface in these nanocomposite magnets. Owing to the

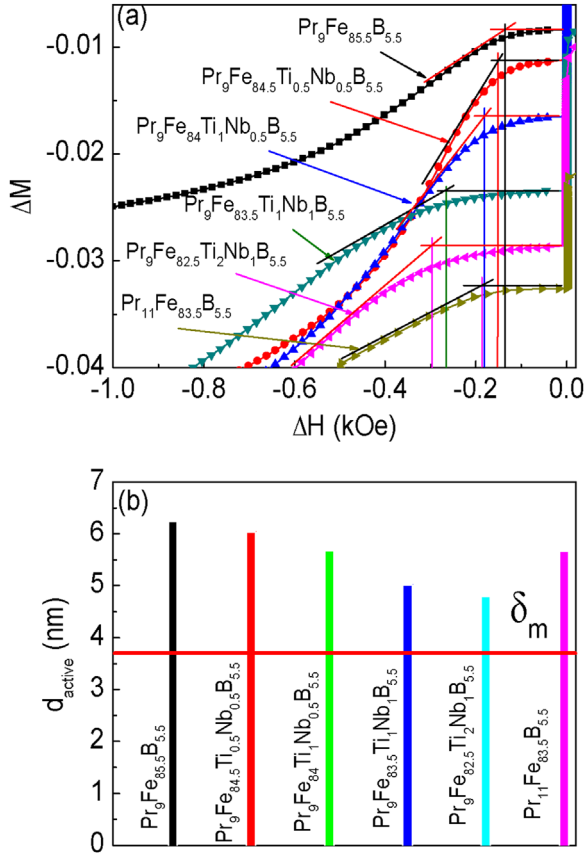


**Fig. 3.** (a) The magnetization behaviors of thermal activation for 1200 s of waiting time at temperature of 300 K. (b) The activation size  $d_{active}$  and ideal domain wall size  $\delta_m$  at temperature of 300 K.

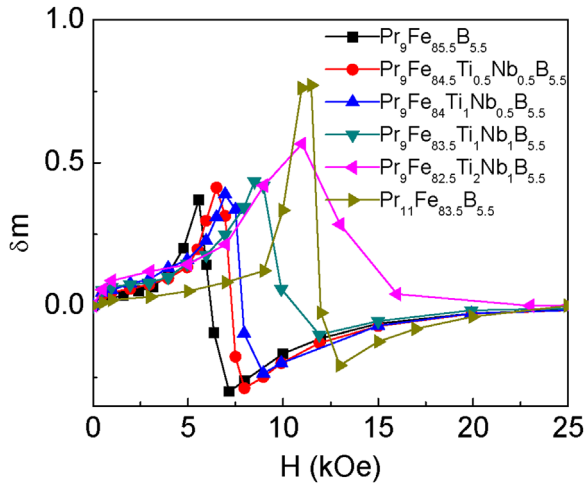


**Fig. 4.**  $\delta m$  curves (Henkel plots) for all samples at temperature of 300 K.

incoherent magnetization reversal, the magnetocrystalline anisotropy energy in hard phase is overcome not only by the Zeeman energy of an applied field and the dipolar interaction energy, but by exchange energy near the interface [22]. The more incoherent magnetization behavior implies high exchange energy in the nucleation of reversed domain wall. Magnetization behavior is more incoherent in high coercivity magnets among these nanocomposites, so the sum of exchange energy and Zeeman energy is larger than that for low coercivity magnets in irreversible magnetization. The doping of TiNb doesn't change magnetocrystalline anisotropy of hard phase and the energy barrier [33], why is the energy

barrier overcome by high exchange energy and Zeeman energy in high coercivity magnets, and why is magnetization reversal more incoherent? It is necessary to make it clearer about the magnetization reversal from soft to hard phase.

Magnetization reversal could be checked by Kronmüller formula,  $\mu_0 H_c(T)/J_s(T) = a_K a_{ex} \mu_0 H_N^{min}(T)/J_s(T) - N_{eff}$  [2,34]. Here microstructure parameter  $a_K$  takes into account the effect of reduced surface magnetocrystalline anisotropy on the coercivity, and  $a_{ex}$  describes the average anisotropy reduced by the exchange coupling effect.  $H_N^{min} = K_1/J_s$ , denoting the ideal nucleation field for isotropic magnets [35].  $N_{eff}$  is an demagnetization factor describing the internal stray fields acting on the grains. As shown in Fig. 5, the coercivity keeps a liner relationship with the ideal nucleation field of  $Pr_2Fe_{14}B$ , suggesting that magnetization reversal undergoes nucleation process of reversed domain in hard phase [35]. In addition,  $N_{eff}$  decreases for the TiNb doping, indicating that internal stray field reduces, leading to the weakening of dipolar effect, which is well consisted with the observation on the negative value of Henkel plots.

As shown in Fig. 5,  $a_K a_{ex}$  value increases for the TiNb addition. Due to the same volume fraction of  $\alpha$ -Fe phase implied in Fig. 1,  $a_{ex}$  is assumed to be the same among these nanocomposites [2,34]. So the difference of  $a_K a_{ex}$  values and coercivities mainly lie in the parameter  $a_K$ , which is similar to that in nanocrystalline magnets [18], indicating that the defect region at hard grain outer-layer and the self-interaction between defect and perfect regions are crucial to the magnetization reversal and coercivity [18]. The perfect hard region bears high magnetocrystalline anisotropy as a skeleton against magnetization reversal in soft phase due to the exchange coupling. However, the existing of defect region changes the nature of exchange coupling. The soft phase is actually exchange-coupled with defect region, and the defect region is coupled with perfect region. In the  $180^\circ$  Bloch wall, the magnetic moments of perfect region part are in the positive direction, and those of defect and soft regions are in the negative direction. Considering with the anisotropy in defect region, the energy density is increased in defect region and approaches to that in perfect hard region in irreversible magnetization. So the magnetocrystalline anisotropy barrier of the perfect hard region is overcome not only by the exchange energy, Zeeman energy and dipolar interaction energy, but also by the anisotropy energy of defect region. The anisotropy in transition region assists magnetization reversal, and therefore it needs a low applied field in the irreversible magnetization.

It was reported that Mo and Ta could inhibit atomic over-diffusion and prevent the deterioration of hard grain boundary [13,36]. Bearing these in mind, refractory elements Ti and Nb may

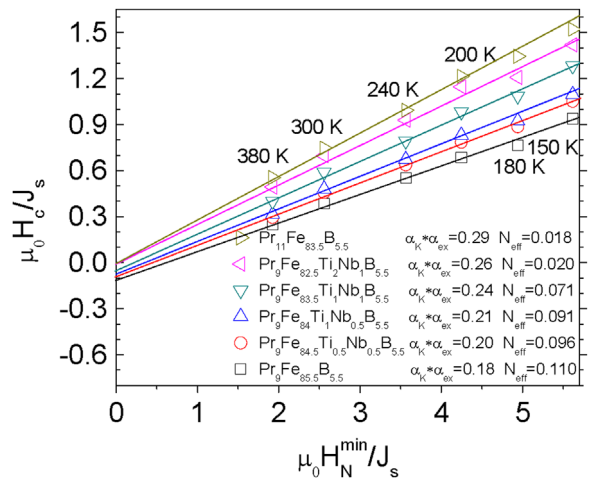


**Fig. 5.** The dependences of  $\mu_0 H_c/J_s$  on  $\mu_0 H_N^{min}/J_s$  for all samples.

mainly aggregate in the tri-junction areas or exist at the interface [14,25], keeping hard grain boundary more perfect, which is the origin of an increase of  $a_K$ . The defect region becomes narrower and the variation of anisotropy from the maximum to zero is abrupt in defect region. So the average energy of reduced anisotropy becomes lower near the perfect region, and there needs to increase the applied field and exchange energy to overcome the energy barrier.

The applied field promotes magnetization reversal in defect region that plays a role as a ladder to overcome the energy barrier. The soft phase also promotes magnetization reversal in defect region by exchange coupling. For nanocomposite  $\text{Pr}_9\text{Fe}_{82.5}\text{Nb}_2\text{Ti}_1\text{B}_{5.5}$ , in irreversible magnetization the exchange energy is higher in defect region compared to that of nanocrystalline  $\text{Pr}_{11}\text{Fe}_{83.5}\text{B}_{5.5}$ , but the coercivity is nearly the same (shown in Fig. 2). This fact is attributed to the effect of soft phase on the magnetization reversal. The soft phase decreases the applied field for reversed domain nucleation in defect region [1], so there needs higher exchange energy to overcome the energy barrier of perfect hard region.

Coercivity is also dependent on the grain size [37]. In micrometer scale grains, if the defect or soft region has large size, the nucleation of reversed domain occurs easily in defect or soft region under a lower applied field, which may promote the reversed domain nucleation in hard region and result in the decrease of coercivity. There are three critical sizes to affect significantly the coercivity [38]. According to the formula  $\delta_m = \pi\sqrt{A/K}$ , the domain wall size  $\delta_m$  in defect or soft region is larger than that of hard phase due to the rather low value of  $K$ . As the grains size decreases to nanoscale less than the domain wall size of the defect or soft region, the nucleation of reversed domain can't occur alone in the defect or soft region, but occurs across the multi-grains by the assisting of the interfacial exchange coupling, so the nucleation field increases. Since the interfacial exchange effect is generally weaker than that inside of gains, it needs higher applied field to promote the nucleation of reversed domain in neighbor grains, which is consistent with the fact that the interface has the pinning effect for the domain wall motion due to the weak intergranular exchange coupling [39]. As the particle size decreases to approach the second critical size, i.e., domain wall size of hard region, the magnetization reversal changes from incoherent to coherent rotation in the isolated particles [37], and the coercivity reaches to a maximum [37,38]. As the grain size further decreases to the

superparamagnetic size, the coercivity declines due to the thermal fluctuation effect.

In the melt-spun ribbons the microstructure is inhomogeneous, the grain size varies from the free surface to near wheel surface, and there exist the amorphous phase, minor phase and soft phase. Due to the well squareness of hysteresis loop, these phases are well exchange-coupled with hard grains in magnetization reversal. Some hard grains have the small crystalline size less than the domain wall size and bear high magnetocrystalline anisotropy. However, due to the exchange coupling with soft or amorphous phase, the nuclei of reversed domain in soft or amorphous phase promote magnetization reversal firstly at hard grain boundary. So magnetization reversal should undergo the nucleation of reversed domain from soft phase to hard phase rather than as that of the isolated particles [37]. The variation of grain size, the interface and the amount of soft and amorphous phase may affect the exchange energy in the nucleation of reversed domain, but doesn't change the mode of magnetization reversal from soft to hard phase.

In addition, the microstructure and domain structure were checked for  $\text{Pr}_9\text{Fe}_{85.5}\text{B}_{5.5}$  and  $\text{Pr}_9\text{Fe}_{82.5}\text{Ti}_2\text{Nb}_1\text{B}_{5.5}$  ribbons using TEM. The grain morphologies are shown in the bright field images of Fig. 6(a) and (b), respectively. There is no much difference in microstructure between the two samples but some grains have larger size in  $\text{Pr}_9\text{Fe}_{85.5}\text{B}_{5.5}$ . The inhomogeneous distribution of grain size could enlarge the dipolar interaction, more or less, resulting in an increase of stray field, which is reason why negative  $\delta m$  and  $N_{\text{eff}}$  are larger in  $\text{Pr}_9\text{Fe}_{85.5}\text{B}_{5.5}$  ribbons. The Fresnel-Lorentz domain structures at over-focus states are shown for the two samples in Fig. 7(a) and (c), respectively. The curved black/white contrast responds to domain wall separated by domains. The domain walls, staying at the hard grain boundary in remanence state, are much more evident in  $\text{Pr}_9\text{Fe}_{85.5}\text{B}_{5.5}$ , which may be ascribed to their larger size and so is well consisted with the observation on the activation size. In addition, as shown by triangles in under-focus state (shown in Fig. 7(b)) and over-focus state of Fig. 7(a), some individual vortex-like spots form mainly at domain boundary in  $\text{Pr}_9\text{Fe}_{85.5}\text{B}_{5.5}$ . These vortex domain structures results from the combined effects of strong intergranular exchange coupling and randomly oriented hard grains [40], which demonstrates the enlarged coupling length near the interface for  $\text{Pr}_9\text{Fe}_{85.5}\text{B}_{5.5}$ .

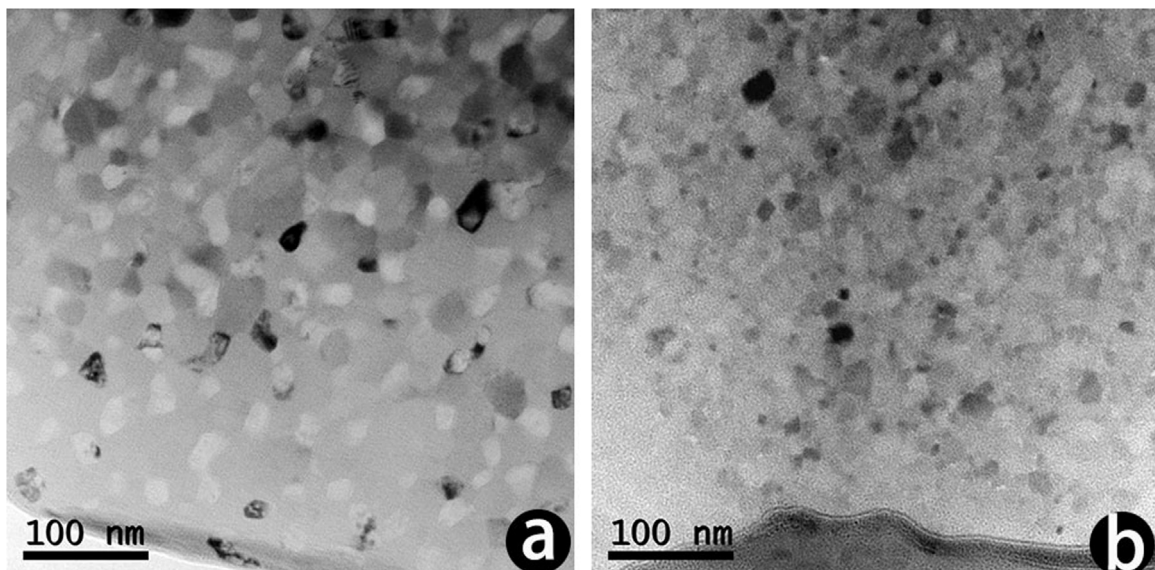
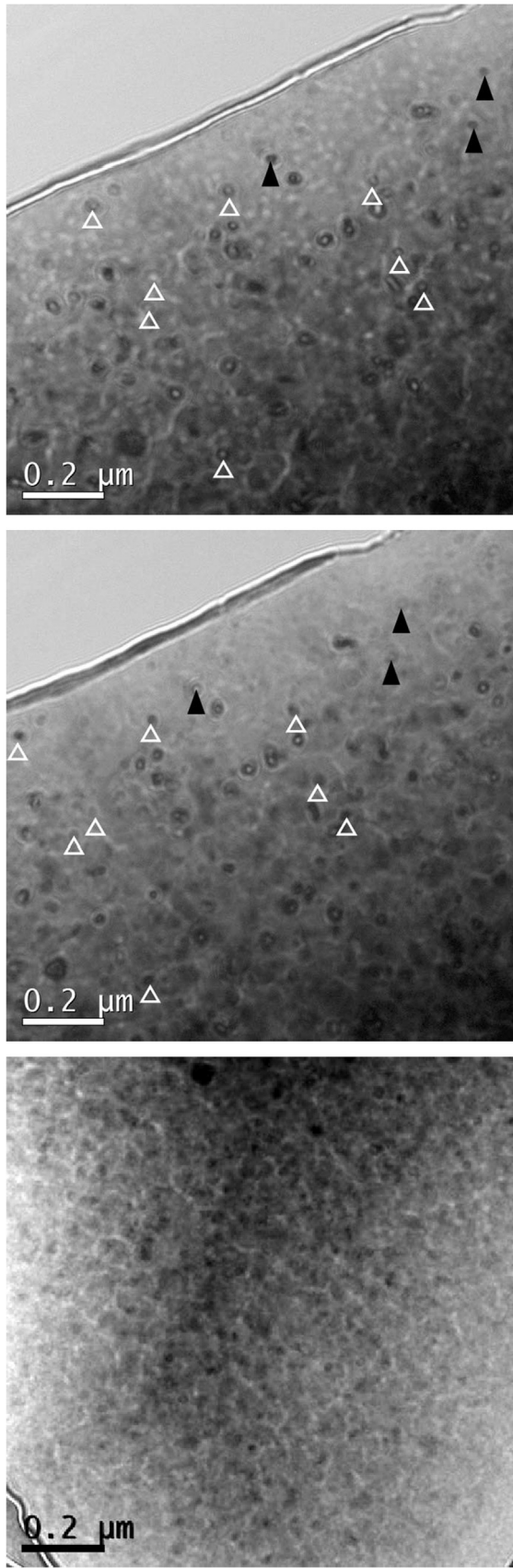


Fig. 6. The bright field images of (a)  $\text{Pr}_9\text{Fe}_{85.5}\text{B}_{5.5}$  ribbon and (b)  $\text{Pr}_9\text{Fe}_{82.5}\text{Ti}_2\text{Nb}_1\text{B}_{5.5}$  ribbon, showing the grain morphology.



**Fig. 7.** The corresponding Fresnel-Lorentz domain structures at (a) over-focus state and (b) under-focus state of  $\text{Pr}_9\text{Fe}_{85.5}\text{B}_{5.5}$  ribbon, and at over-focus state of (c)  $\text{Pr}_9\text{Fe}_{82.5}\text{Ti}_2\text{Nb}_1\text{B}_{5.5}$  ribbon.

#### 4. Conclusions

In summary, the domain wall size is investigated by the measurement of thermal activation in  $\text{Pr}_2\text{Fe}_{14}\text{B}/\alpha\text{-Fe}$  magnets. It proposes that the domain wall involves a little part defect region and that the soft phase is exchange-coupled with the defect region rather than with the perfect hard region. The magnetocrystalline anisotropy of perfect hard region is overcome not only by the exchange energy and Zeeman energy, but by the anisotropy energy in defect region. The soft phase assists magnetization reversal in defect region by exchange coupling, and the defect region increases the anisotropy energy in negative direction of domain wall to overcome the energy barrier. The diminishing of defect region is beneficial to reduce the anisotropy energy in negative direction of domain wall and to increase the coercivity.

#### Acknowledgments

The present work was supported by the National Basic Research Program of China (Grant no. 2014CB643702), and the National Natural Science Foundation of China (Grant no. 51461033, 51590880).

#### References

- [1] R. Skomski, J.M.D. Coey, *Phys. Rev. B* 48 (1993) 15812.
- [2] J. Bauer, M. Seeger, A. Zern, H. Kronmüller, *J. Appl. Phys.* 80 (1996) 1667.
- [3] W. Liu, Z.D. Zhang, J.P. Liu, L.J. Chen, L.L. He, Y. Liu, X.K. Sun, D.J. Sellmyer, *Adv. Mater.* 14 (2002) 1832.
- [4] W. Si, G.P. Zhao, N. Ran, Y. Peng, F.J. Morvan, X.L. Wan, *Sci. Rep.* 5 (2015) 16212.
- [5] A.M. Gabby, Y. Zhang, G.C. Hadjipanayis, *Appl. Phys. Lett.* 85 (2004) 446.
- [6] G.B. Han, R.W. Gao, S. Fu, W.C. Feng, H.Q. Liu, W. Chen, W. Li, Y.Q. Guo, *Appl. Phys. A* 81 (2005) 579.
- [7] G.P. Zhao, M.G. Zhao, H.S. Lim, Y.P. Feng, C.K. Ong, *Appl. Phys. Lett.* 87 (2005) 162513.
- [8] H. Kronmüller, D. Goll, *Phys. Status Solidi B* 248 (2011) 2361.
- [9] W. Liu, X.H. Liu, W.B. Cui, W.J. Gong, Z.D. Zhang, *Chin. Phys. B* 22 (2013) 027104.
- [10] X.Y. Zhang, Y. Guan, J.W. Zhang, *Appl. Phys. Lett.* 80 (2002) 1966.
- [11] Y. Choi, J.S. Jiang, J.E. Pearson, S.D. Bader, J.J. Kavich, J.W. Freeland, J.P. Liu, *Appl. Phys. Lett.* 91 (2007) 072509.
- [12] R. Larde, J.M.L. Breton, A. Maître, D. Ledue, O. Isnard, V. Pop, I. Chicas, *J. Phys. Chem. C* 117 (2013) 7801.
- [13] W.B. Cui, S.J. Zheng, W. Liu, X.L. Ma, F. Yang, Q. Yao, X.G. Zhao, Z.D. Zhang, *J. Appl. Phys.* 104 (2008) 053903.
- [14] H. Li, L. Lou, F. Hou, D. Guo, W. Li, X. Li, D.V. Gunderov, K. Sato, X. Zhang, *Appl. Phys. Lett.* 103 (2013) 142406.
- [15] Y. Choi, J.S. Jiang, Y. Ding, R.A. Rosenberg, J.E. Pearson, S.D. Bader, A. Zambano, M. Murakami, I. Takeuchi, Z.L. Wang, J.P. Liu, *Phys. Rev. B* 75 (2007) 104432.
- [16] J. Zhang, Y.K. Takahashi, R. Gopalan, K. Hono, *Appl. Phys. Lett.* 86 (2005) 122509.
- [17] R.W. Gao, D.H. Zhang, H. Li, S.T. Jiang, S.Z. Zhou, F.B. Li, L.D. Zhang, *J. Appl. Phys.* 78 (1995) 1156.
- [18] Z.B. Li, B.G. Shen, M. Zhang, Y. Zhang, F.X. Hu, J.R. Sun, *Appl. Phys. Lett.* 106 (2015) 042403.
- [19] D. Givord, M. Rossignol, V.M.T.S. Barthem, *J. Magn. Magn. Mater.* 258–259 (2003) 1.
- [20] S.L. Chen, W. Liu, Z.D. Zhang, *Phys. Rev. B* 72 (2005) 224419.
- [21] J.P. Bick, D. Honecker, F. Döbrich, K. Suzuki, E.P. Gilbert, H. Frielinghaus, J. Kohlbrecher, J. Gavilano, E.M. Forgan, R. Schweins, P. Lindner, R. Birringer, A. Michels, *Appl. Phys. Lett.* 102 (2013) 022415.
- [22] R. Fischer, H. Kronmüller, *J. Magn. Magn. Mater.* 191 (1999) 225.
- [23] E.P. Wohlfarth, *J. Phys. F: Met. Phys.* 14 (1984) L155–L159.
- [24] H. Kronmüller, M. Fahnle, *Micromagnetism and the Microstructure of Ferromagnetic Solids*, Cambridge University Press 2003, p. 420.
- [25] H.W. Chang, C.H. Chiu, C.W. Chang, W.C. Chang, A.C. Sun, Y.D. Yao, *Scr. Mater.* 55 (2006) 529.
- [26] Z.B. Li, B.G. Shen, E. Niu, R.M. Liu, M. Zhang, J.R. Sun, *Chin. Phys. B* 22 (2013) 117503.
- [27] V. Neu, C. Schulze, M. Faustini, J. Lee, D. Makarov, D. Suess, S.-K. Kim, D. Grosso, L. Schultz, M. Albrecht, *Nanotechnology* 24 (2013) 145702.
- [28] D. Givord, P. Tenaud, T. Viadieu, *IEEE Trans. Magn.* 24 (1988) 1921.

- [29] H.W. Zhang, C.B. Rong, J. Zhang, S.Y. Zhang, B.G. Shen, Phys. Rev. B 66 (2002) 184436.
- [30] J.P. Attané, D. Ravelosona, A. Marty, Y. Samson, C. Chappert, Phys. Rev. Lett. 96 (2006) 147204.
- [31] P.E. Kelly, K. O'Grady, P.I. Mayo, R.W. Chantrell, IEEE Trans. Magn. 25 (1989) 3881.
- [32] Z.B. Li, M. Zhang, B.G. Shen, J.R. Sun, Appl. Phys. Lett. 102 (2013) 102405.
- [33] R. Goto, S. Okamoto, N. Kikuchi, O. Kitakami, J. Appl. Phys. 117 (2015) 17B514.
- [34] D. Goll, M. Seeger, H. Kronmüller, J. Magn. Magn. Mater. 185 (1998) 49.
- [35] H. Kronmüller, K.-D. Durst, M. Sagawa, J. Magn. Magn. Mater. 74 (1988) 291.
- [36] W.B. Cui, Y.K. Takahashi, K. Hono, Adv. Mater. 24 (2012) 6530.
- [37] T. Shima, K. Takanashi, Y.K. Takahashi, K. Hono, Appl. Phys. Lett. 81 (2002) 1050.
- [38] X.C. Liu, R. Xie, J. Pan, Trans. Nonferrous Met. Soc. China 19 (2009) 1131.
- [39] Z.B. Li, B.G. Shen, E. Niu, J.R. Sun, Appl. Phys. Lett. 103 (2013) 062405.
- [40] Y. Gao, D. Shindo, A.K. Petford-Long, J. Appl. Phys. 93 (2003) 8119.